

Far-infrared emission as a tracer for star formation in nearby molecular clouds

23/03/2023

Mohammed Safeer Zaheer (20014777)

Course: PHAS0113

Project supervisor: Dr. Kate Pattle

Group: B

Abstract

The main aim of this project is to study the mass distribution of a nearby molecular cloud to generate an equation (core-mass function or CMF) that fairly accurately models the mass distributions in the cloud. We further aim to compare the CMF to initial-mass functions (IMF) to gain a better understanding of how stars evolve as they form. The data for this project was of the Ophiuchus molecular cloud taken by the JCMT's SCUBA-2 camera in Mauna Kea. The observations were done in 850 microns (Far-IR) to avoid atmospheric effects. All the observation data can be found in Canadian Astronomy Data Centre (CADC)'s archive. We enacted the use of source-extraction algorithms to identify pre-stellar cores in the data and generate a catalog of their data. We then generated a histogram of their masses, modelling a function over a characteristic region in the distribution that is well-approximated by a power-law. Assuming a cloud-temperature of 15K, we get a power-law relation of the form:

$$y = (0.791 \pm 0.132) \cdot M^{(-0.726 \pm 0.227)}$$

After calculating our power-law relation, we then compared our results to results for the small molecular cloud found in other papers.

Introduction and Theory

Archival data from JCMT's SCUBA-2 was procured via the CADC. The data was originally taken for the Gould Belt Survey . One of the main aims of the survey was to investigate formation of low-mass stars in nearby molecular clouds. The observations were done in 850 microns, which falls in the far-infrared region. This wavelength was chosen due to 2 reasons: the cold, dark clouds emit in the infrared and not visible; and the atmosphere, which is usually opaque in IR, is relatively transparent in this regime (along with 450 microns IR).

In this project, we aimed to study the distribution of pre-stellar cores in a nearby molecular cloud. A pre-stellar core is a clump of gas and dust with a density greater than the surrounding molecular cloud due to gravitational collapse. These are precursors to newly formed stars, which means that studying them can give insight on how the IMF and CMF are related. The IMF is made by studying the distribution of stellar masses, while the CMF is made by studying the cores that aren't necessarily stars yet, but are a necessary path to stellar formation. Thus, comparing these two can give good insight into the efficiencies and intricacies of star-birth. The IMF and CMF both have very similar shapes; they display a power-law for higher mass stars and a log-normal for lower mass stars (Salpeter, 1955; Chabrier, 2003).

To obtain a CMF, we will used a source-extraction algorithm called ‘Astrodendro’ to pick out pre-stellar cores in the data via contour-mapping. And once we obtained a catalog of the cores and their fluxes, we then computed a histogram of their mass distributions, with the mass being calculated from the flux via the Dust-Mass equation,

$$M = \frac{F_\nu \cdot D^2}{B_\nu(T) \cdot \kappa_\nu}$$

where M is the mass of the object, F_ν is the monochromatic flux of the object, D is the distance to the object, $B_\nu(T)$ is the planck function and κ_ν is the dust opacity. Next, we fit a power-law to the higher-mass end of the distribution to obtain our power-law slope, which will then be compared to other papers' values to see how we did. Finally, we compared an IMF to our CMF to see what kind of changes occur as stars evolve.

Target

The ideal target for our project was a nearby molecular cloud (<500 pc away to be included in Gould Belt Survey) with a big enough angular size in the sky and sufficiently many cores in it. But the cloud can't be too big either, as extending the field of view too wide would be a problem for the JCMT. Finally, the cloud also had to have been observed by the JCMT already. Thus, keeping all these parameters in mind, we chose the Ophiuchus molecular cloud as our target for the group project. It is much closer to us than most of the other clouds imaged by the Gould Belt Survey at only 139 ± 6 pc from us (Mamajek, 2008). It is also very helpful that Ophiuchus has a litany of literature that can be used to assume values for parameters that we do not directly measure ourselves. We will be

specifically looking at the clouds L1688 and L1689, which are both star forming regions in the cloud complex. This means there should be a lot of pre-stellar cores in this region, which is helpful in increasing sample size for our histogram.

Data Acquisition

The table below shows the required data to find the images of our target on the CADC's archive^[1].

Table 1: Information about Ophiuchus that was used to look for relevant data in CADC archive.

Name (Target ID):	Rho Ophiuchi cloud complex
Proposal ID:	MJLSG32
Right Ascension:	16h 28m 06s
Declination:	- 24° 32' 30.2"
Distance from Sun:	(139 ± 6) pc or (4.29 ± 0.18) 10 ¹⁸ m
Observation Filter:	SCUBA-2 observes in 850 μ m wavelength

Using this data, we were able to find multiple observations of our target on the archive. Having already calculated our mass sensitivity limit (which will be discussed later), Noah and I then used JCMT's Integration Time Calculator (ITC)^[2] to find out if the observation data reached our standards for this project. One such standard was that the data should have lower mass sensitivity than the mass of a brown dwarf (including a 3 σ rating). Noah, using the Dust-Mass equation, calculated the flux sensitivity required to be 0.0228 Jy = 2.28 x 10⁻²⁸ W Sr⁻¹ Hz⁻¹. Here we assumed the values: T = 15K, distance is same as above. κ_ν was calculated using the equation:

$$\kappa_\nu = \kappa_o \cdot \left(\frac{\nu}{\nu_o}\right)^\beta = 0.1 \left(\frac{cm^2}{g}\right) \times \left(\frac{\nu}{1THz}\right)^{1.8}$$

κ_o , ν_o values were obtained from (Beckwith et al, 1990), and β from (Planck Collaboration XXV 2011; Martin et al. 2013).

We found out that the data in general had a mass sensitivity much lower than what we required, meaning that the observation data was usable. We also ensured that the data was taken in Band 1 or 2 weather (transmission of 82% and 77% respectively^[3]) to ensure that our data was of good quality. Although Band 1 weather is preferable, it is very rare, and thus, Band 2 is an acceptable compromise. In our project, the mapping mode of the observation also matters a lot. For our case, two types of mappings were available: PONGs or DAISYs (comparison can be seen in Appendix 1). While DAISYs have great sensitivity at the center of the map (useful for singular objects), PONGs have a much more spread out area of mapping, which is much better for large-field observations as important objects need not necessarily be in the center for these cases. The telescope array, in this mode, is bounced around the field, resulting in nice flat noise throughout most of the field, giving an evenly based set of observations (Holland, 2013). We requested for data taken via PONG1800s, with '1800' corresponding to the

diameter of the map in arcseconds. We need this wide-field due to the disperse nature of the molecular cloud, even though the pre-stellar cores themselves are point objects.

Data Reduction

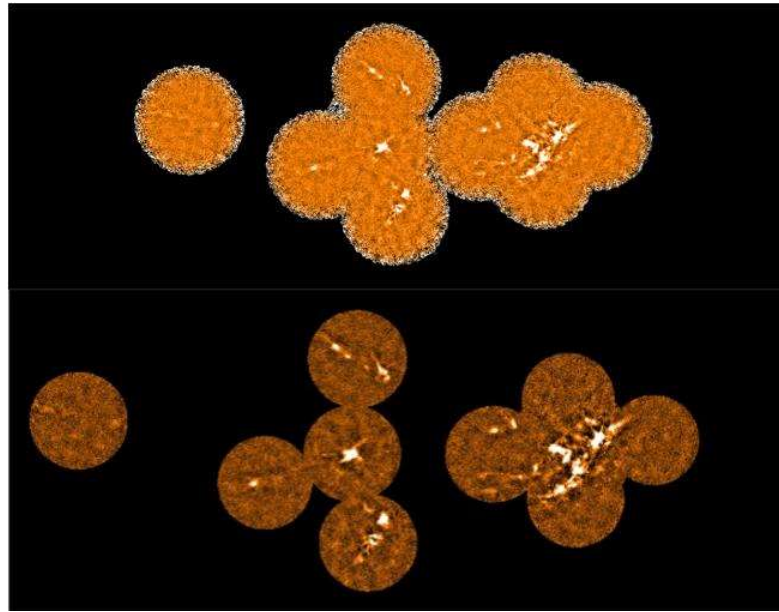


Fig 1: Top image is of log-scale plot of our data, with black-white edges being areas of high noise. Bottom image is of the same field, but noisy areas are cut off.

Although the image in general has a flat noise level due to it being a mosaic of PONG-maps, the edges of each mosaic have a lot more noise than everywhere else on the field (this can be seen at the edges of circles in figure 1). This is an artifact of how PONG operates. Thus, Scarlett enlisted the use of GAIA imaging software to cut off these noisy regions. First we displayed the image in log-scale to be able to identify areas of noise. Next, we used circular apertures to slice those areas out, leaving the flat-noise regions in the image for further use.

The data was given to us reduced, which means that besides the noise we removed above due to mapping mode, all other noise-sources were reduced for us before we received the data. This was done via iterative routine of ‘makemap’, which comes as a part of the ‘Smurf’ package (Kirk et al., 2018).

Data Analysis and Results

Scarlett also analyzed the standard deviation (or the RMS) in the image using GAIA. In GAIA, ‘Image analysis’ can calculate this for you using apertures. We used apertures of constant at areas where flat field noise dominates

and made measurements over 100 times to get a standard deviation of $0.0593 \text{ mJy} \cdot \text{arcs}^{-2}$. Please note that this was done on the noisy version of the data (imaged in Top-image of figure 1).

A source-extraction algorithm is needed to count the pre-stellar cores to make our calculations reproducible. The source-extraction algorithm we used is called ‘Astrodendro’[5]. This algorithm is a python package which generates contour maps of your images based on flux values. These are then used to generate a dendrogram (example can be seen in Appendix 2). Counting the ‘leaves’ in the dendrogram gives us the number of cores.

This algorithm is parametrized by: the minimum value to be detected, the minimum dip required to classify two peaks as actually being two peaks, and the minimum size of a source (dependent on the minimum beam size as object is a point-source, which is further dependent upon the resolution of the telescope). The minimum value to be detected is calculated using our standard deviation from Gaia and the target SNR of our results. We wanted a 3-sigma accuracy, and thus used $3 \times \text{standard-deviation}$ as our minimum value. The minimum dip (also called minimum delta) was decided by running the algorithm on a highly populated region in the image and seeing which values of minimum delta give the best core-recognition. We decided on a minimum delta value of 3σ . The npix value was calculated by using the telescope’s resolution-dependent beam-width of 14.3 arcsecs along with the fact that each pixel has length of 3 arcseconds in the image^[3] to get a minimum size of source of about 25 pixels^[5]. I ran the algorithm on the whole image with the parameters above, giving us the dendrogram seen in Appendix 3.

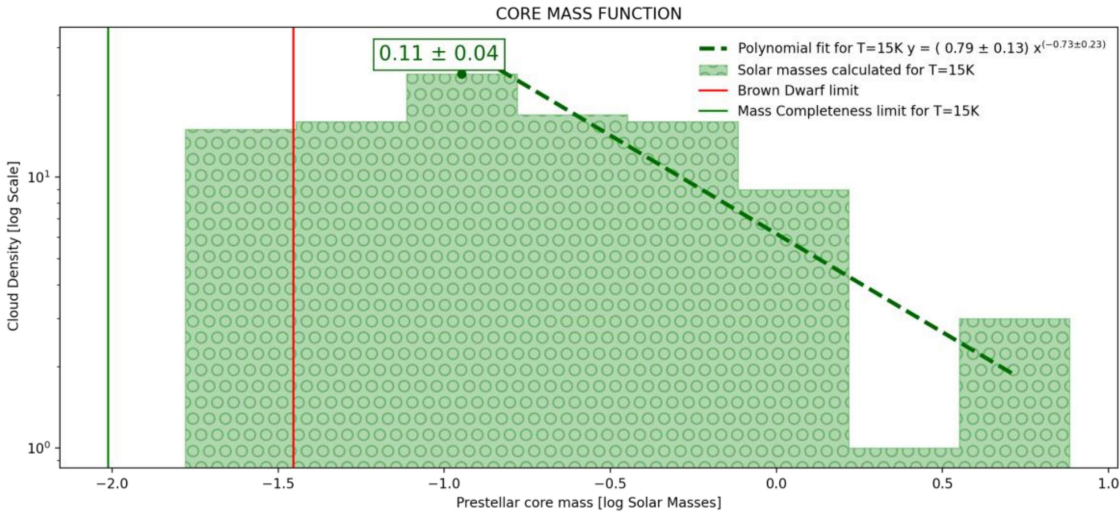


Figure 2: Log-scale Histogram of masses along with power-law model (dotted line).

These cores were then cataloged. A catalog of the cores along with some associated values can be found at the end of this section. Finally, using the flux values of these cores along with the Dust-Mass equation , Noah then created a histogram of mass distribution of pre-stellar cores in the Ophiuchus cloud. The histogram had masses ranging from 0.02 to 7.64 solar masses. Since the histograms are best presented in a log-scale, we thought it best

to make all the data logarithmic and try to fit a line of best fit, giving us a power-law's slope. Using the values in the histogram in conjunction with np.polyfit in python, we get a polynomial fit of:

$$N = (0.791 \pm 0.132) \cdot M^{(-0.726 \pm 0.227)}$$

Table 2: Comparing our CMF against CMF calculated for the same region in different papers.

(1 mJy = 10^{-29} W Sr $^{-1}$ Hz $^{-1}$)

Idx	RA (Degrees)	Dec (Degrees)	Exact Area (Pixel count)	Flux (mJy)	dF (mJy)	Mass (M \odot)	dM (M \odot)
1	248.05	-25.06	349	845.84	84.58	0.44	0.04
2	248.07	-25.05	364	894.14	89.41	0.46	0.05
3	248.02	-25.01	119	259.49	25.95	0.13	0.01
4	248.01	-25.00	125	298.37	29.84	0.15	0.02
5	247.99	-24.96	841	4831.73	483.17	2.49	0.25
6	248.02	-24.96	157	387.31	38.73	0.20	0.02
7	248.04	-24.94	173	393.87	39.39	0.20	0.02
8	248.00	-24.95	65	471.11	47.11	0.24	0.02
9	247.97	-24.93	459	2773.16	277.32	1.43	0.14
10	247.95	-24.94	157	595.89	59.59	0.31	0.03
11	248.00	-24.93	85	374.71	37.47	0.19	0.02
12	247.93	-24.92	31	68.42	6.84	0.04	0.00
13	247.90	-24.88	76	200.35	20.04	0.10	0.01
14	247.94	-24.85	141	794.45	79.45	0.41	0.04
15	247.92	-24.83	1924	17509.30	1750.93	9.00	0.90
16	248.01	-24.78	723	1665.14	166.51	0.86	0.09
17	246.74	-24.76	70	437.57	43.76	0.23	0.02
18	246.94	-24.75	207	455.95	45.59	0.23	0.02
19	246.60	-24.72	62	440.45	44.05	0.23	0.02
20	246.92	-24.72	33	154.89	15.49	0.08	0.01
21	246.92	-24.71	247	911.18	91.12	0.47	0.05
22	248.48	-24.70	41	137.33	13.73	0.07	0.01
23	246.85	-24.68	67	937.70	93.77	0.48	0.05
24	246.86	-24.68	49	730.06	73.01	0.38	0.04
25	246.80	-24.68	33	88.36	8.84	0.05	0.00
26	246.84	-24.67	45	566.81	56.68	0.29	0.03
27	246.87	-24.66	152	718.55	71.86	0.37	0.04
28	246.79	-24.66	161	779.47	77.95	0.40	0.04
29	248.70	-24.63	1641	5721.73	572.17	2.95	0.29
30	246.77	-24.65	442	2826.98	282.70	1.46	0.15
31	246.91	-24.65	26	75.85	7.59	0.04	0.00
32	246.81	-24.64	68	215.62	21.56	0.11	0.01

33	246.78	-24.64	105	437.53	43.75	0.23	0.02
34	246.80	-24.63	131	516.12	51.61	0.27	0.03
35	246.74	-24.63	244	648.52	64.85	0.33	0.03
36	246.79	-24.62	131	888.98	88.90	0.46	0.05
37	246.78	-24.62	25	137.55	13.75	0.07	0.01
38	247.07	-24.62	35	141.81	14.18	0.07	0.01
39	247.09	-24.61	526	1930.24	193.02	1.00	0.10
40	246.73	-24.61	112	252.64	25.26	0.13	0.01
41	246.77	-24.61	89	481.20	48.12	0.25	0.02
42	247.32	-24.60	142	311.34	31.13	0.16	0.02
43	246.74	-24.57	3606	25474.14	2547.41	13.12	1.31
44	246.91	-24.59	59	120.32	12.03	0.06	0.01
45	246.69	-24.58	157	482.27	48.23	0.25	0.02
46	247.00	-24.56	1021	4553.14	455.31	2.35	0.23
47	246.61	-24.56	569	1222.74	122.27	0.63	0.06
48	246.69	-24.56	152	380.67	38.07	0.20	0.02
49	246.51	-24.54	120	291.36	29.14	0.15	0.02
50	246.74	-24.53	1020	4454.69	445.47	2.30	0.23
51	246.97	-24.53	52	115.29	11.53	0.06	0.01
52	246.51	-24.52	87	197.17	19.72	0.10	0.01
53	246.81	-24.51	169	2199.49	219.95	1.13	0.11
54	246.91	-24.51	29	86.08	8.61	0.04	0.00
55	248.06	-24.50	303	922.80	92.28	0.48	0.05
56	246.69	-24.49	670	1999.43	199.94	1.03	0.10
57	246.80	-24.49	207	2709.16	270.92	1.40	0.14
58	248.12	-24.48	323	10323.30	1032.33	5.33	0.53
59	248.10	-24.48	404	31420.65	3142.07	16.19	1.62
60	246.83	-24.48	112	559.22	55.92	0.29	0.03
61	246.89	-24.48	55	158.94	15.89	0.08	0.01
62	247.19	-24.47	33	96.57	9.66	0.05	0.00
63	246.58	-24.47	30	124.93	12.49	0.06	0.01
64	247.89	-24.46	36	124.84	12.48	0.06	0.01
65	246.80	-24.46	137	722.79	72.28	0.37	0.04
66	246.83	-24.45	109	1146.91	114.69	0.59	0.06
67	246.87	-24.45	169	4119.62	411.96	2.12	0.21
68	246.86	-24.45	49	1078.87	107.89	0.56	0.06
69	246.67	-24.45	41	179.18	17.92	0.09	0.01
70	246.76	-24.44	191	416.09	41.61	0.21	0.02
71	246.89	-24.44	148	3065.37	306.54	1.58	0.16
72	246.68	-24.43	187	475.47	47.55	0.24	0.02
73	246.64	-24.44	52	442.12	44.21	0.23	0.02

74	246.56	-24.42	305	1392.64	139.26	0.72	0.07
75	246.62	-24.40	2294	77823.77	7782.38	40.12	4.01
76	246.58	-24.42	37	148.72	14.87	0.08	0.01
77	246.84	-24.41	50	110.15	11.01	0.06	0.01
78	246.70	-24.40	99	223.61	22.36	0.12	0.01
79	246.74	-24.39	594	1394.30	139.43	0.72	0.07
80	246.57	-24.40	49	163.83	16.38	0.08	0.01
81	246.54	-24.39	145	507.41	50.74	0.26	0.03
82	246.69	-24.39	56	484.51	48.45	0.25	0.02
83	246.59	-24.38	146	2161.54	216.15	1.12	0.11
84	246.41	-24.38	36	131.19	13.12	0.07	0.01
85	247.25	-24.35	1303	4969.20	496.92	2.56	0.26
86	246.54	-24.34	841	4865.17	486.52	2.51	0.25
87	246.54	-24.35	56	429.59	42.96	0.22	0.02
88	246.48	-24.35	25	76.87	7.69	0.04	0.00
89	246.59	-24.33	120	306.43	30.64	0.16	0.02
90	247.13	-24.31	1410	4947.22	494.72	2.55	0.25
91	246.73	-24.32	537	1282.54	128.25	0.66	0.07
92	246.49	-24.32	462	1624.81	162.48	0.84	0.08
93	246.79	-24.32	46	247.16	24.72	0.13	0.01
94	246.65	-24.30	551	2295.96	229.60	1.18	0.12
95	246.68	-24.29	510	2932.71	293.27	1.51	0.15
96	246.60	-24.27	69	637.21	63.72	0.33	0.03
97	247.89	-24.05	544	1736.38	173.64	0.89	0.09
98	247.90	-24.02	483	2843.97	284.40	1.46	0.15
99	247.93	-24.01	533	2431.93	243.19	1.25	0.13
100	248.01	-23.99	198	440.22	44.02	0.23	0.02
101	248.12	-23.93	679	2279.30	227.93	1.18	0.12
102	248.20	-23.88	1770	6481.59	648.16	3.34	0.33

Error Analysis

There are four values which we have propagated errors for in this project: the two values associated with the polynomial fit, the flux values for cores generated by the Astrodendro catalog, and the masses calculated for the cores in the catalogs.

We used `np.polyfit` to generate the straight line fit for the log-hist plot, and in `np.polyfit`, there is a parameter called ‘cov’, which when set true, also generates a covariance matrix. Taking the square-root of the matrix’s diagonal gives us the uncertainties in the two parameters in our power-law.

For the uncertainty in the cores’ flux values, I used the following equation:

$$dF = \sqrt{(0.1 \cdot Flux)^2 + (\sigma \cdot \sqrt{N_{pix}})^2}$$

Here, σ is the standard deviation calculated in the data analysis section, N_{pix} is the number of pixels in the core, and the factor of 0.1 comes from the calibration error here being 10% of the flux (Dempsey et al, 2013). The equation for dF is the quadrature sum of calibration error and systematic uncertainty. Finally, the uncertainty in mass was calculated using the relative uncertainty in the flux value, as they are related linearly via the dust-mass equation.

Conclusions

Table 3: Comparing our CMF against CMF calculated for the same region in different papers.

	Our CMF (T=15K, 2023)	Pattle et al. (T=13.5K, 2015)	Sadavoy et al. (T=15K, 2010)
Polynomial Slope:	-0.726 ± 0.227	-1.0 ± 0.4	-1.26 ± 0.20
Core mass range:	$0.02 M_{\odot} > M > 7.64 M_{\odot}$	$M > 0.2 M_{\odot}$	$M > 0.5 M_{\odot}$
Completeness limit:	$0.01 M_{\odot}$	80% completeness limit of $0.051 M_{\odot}$	n/a
Peak:	$0.11 \pm 0.04 M_{\odot}$	$0.1 M_{\odot}$	$0.1 M_{\odot}$

Looking at the table's last row, we can see that all three papers agree on where the peak in the mass distribution lies. But there are differences in the results from the polynomial slopes. Our CMF seems to agree with Pattle et al.'s CMF, as their uncertainties overlap, but these two papers have assumed slightly different values for temperature (15K and 13.5K). On the other hand, Sadavoy et al. Assumes the same temperature as us, but ends with values that do not overlap. All things considered; our results seem to align with Pattle et al. Considering the fact that our temperature values were chosen via eye-based approximation rather than statistical analysis of temperature maps of Ophiuchus. Altering our assumed temperature would only shift the histograms and the power-law on the x-axis, maintaining the same slope regardless of temperature. Although the results could have been more thorough, especially in the case of determining the temperature and beta-values used in the Mass-Dust equation, the CMF achieved in the end was quite similar to the ones found in other papers. Also, the peak of the distribution was also well in agreement with previous CMF attempts on this cloud. We also managed to catalog a lot of the cores from the data provided to us.

There could have been a major noise source from the way makemap reduces data (Helen et al., 2018). If the initial conditions are not well-selected, could lead to false structure forming in the image as iterations go exponentially wrong.

One way to fix some of the problems in this project would have been to critically look at the assumptions we made in this project, like the values assumed. Also would have liked to run the data through more algorithms, like SExtractor, given more time. Finally, would have liked to conduct a full-depth comparison of an IMF of this region against our CMF to under their statistical relation.

My main learning point in this project has been the use of various softwares, including software packages I'd had never heard of. Its been especially interesting knowing how to use python in increasingly interesting ways to get the data that we need. Another important takeaway for me learning how to cite well. Although I know how to cite, keeping a concious mind about always looking for evidence for the assumptions you make in a project.

Appendix

1 PONG vs DAISY map

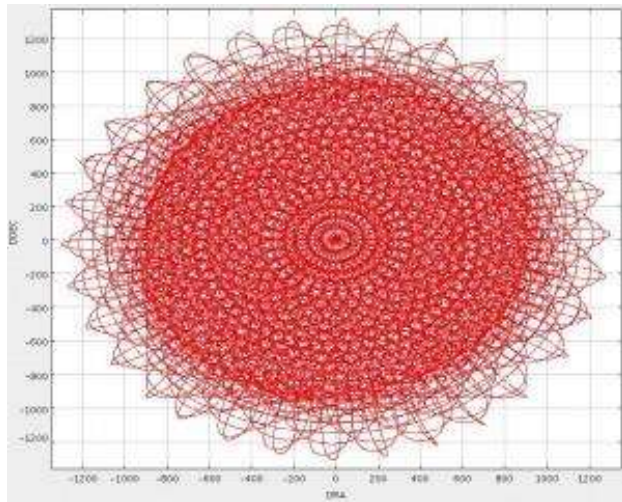


Figure 3: PONG1800 map.

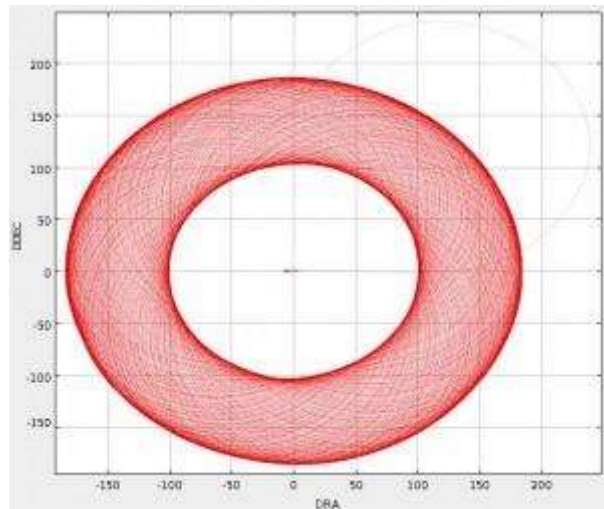


Figure 4: DAISY map.

2 Dendrogram example

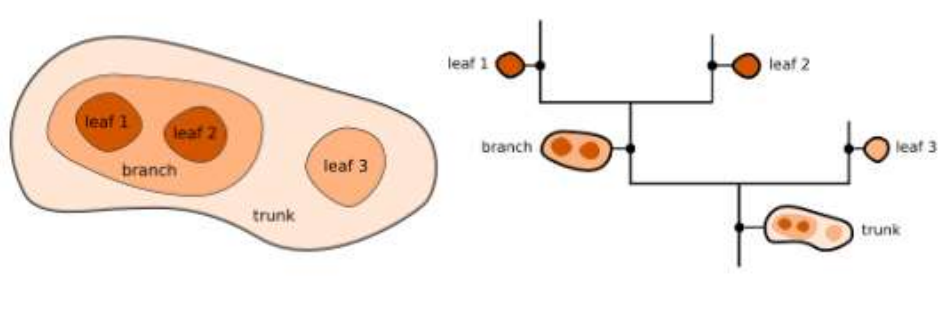


Figure 5: How a contour map correlates to a dendrogram.

Here we can see how a simplified contour map of a molecular cloud is interpreted as a dendrogram.

3 Dendrogram of full image

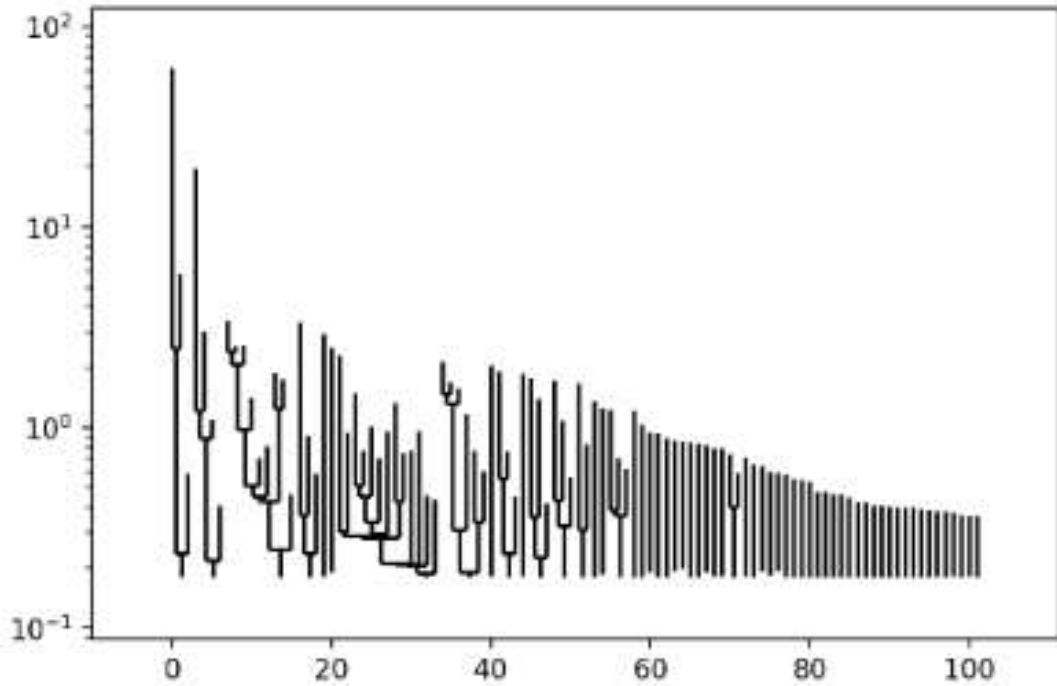


Figure 6 : Dendrogram of the whole data of image. Here, x-axis represents index of core, while y-axis represents flux.

Bibliography

Sources

- Chabrier, Gilles. “Galactic Stellar and Substellar Initial Mass Function.” *Publications of the Astronomical Society of the Pacific*, vol. 115, no. 809, 2003, pp. 763–795., doi:10.1086/376392.
- Salpeter, Edwin E. “The Luminosity Function and Stellar Evolution.” *The Astrophysical Journal*, vol. 121, 1955, p. 161., doi:10.1086/145971.
- Holland, W. S., et al. “Scuba-2: The 10 000 Pixel Bolometer Camera on the James Clerk Maxwell Telescope.” *Monthly Notices of the Royal Astronomical Society*, vol. 430, no. 4, 2013, pp. 2513–2533., doi:10.1093/mnras/sts612.
- Beckwith, Steven V. W., et al. “A Survey for Circumstellar Disks around Young Stellar Objects.” *The Astronomical Journal*, vol. 99, Mar. 1990, p. 924, doi:<https://doi.org/10.1086/115385>.
- Abergel, A., et al. “Planck Early Results. XXV. Thermal Dust in Nearby Molecular Clouds.” *Astronomy & Astrophysics*, vol. 536, 2011, doi:10.1051/0004-6361/201116483.
- Kirk, Helen, et al. “The JCMT Gould Belt Survey: SCUBA-2 Data Reduction Methods and Gaussian Source Recovery Analysis.” *The Astrophysical Journal Supplement Series*, vol. 238, no. 1, Sept. 2018, p. 8, doi:<https://doi.org/10.3847/1538-4365/aada7f>.
- Dempsey, J. T., et al. “SCUBA-2: On-Sky Calibration Using Submillimetre Standard Sources.” *Monthly Notices of the Royal Astronomical Society*, vol. 430, no. 4, Mar. 2013, pp. 2534–44, doi:<https://doi.org/10.1093/mnras/stt090>.
- Pattle, K., et al. “The JCMT Gould Belt Survey: First Results from the SCUBA-2 Observations of the Ophiuchus Molecular Cloud and a Virial Analysis of Its Prestellar Core Population.” *Monthly Notices of the Royal Astronomical Society*, vol. 450, no. 1, Apr. 2015, pp. 1094–122, doi:<https://doi.org/10.1093/mnras/stv376>.
- Beckwith, Steven V. W., et al. “A Survey for Circumstellar Disks around Young Stellar Objects.” *The Astronomical Journal*, vol. 99, Mar. 1990, p. 924, doi:<https://doi.org/10.1086/115385>.

References

- [1] CADC (n.d.). *Advanced Search*. [online] www.cadc-ccda.hia-iha.nrc-cnrc.gc.ca. Available at: <https://www.cadc-ccda.hia-iha.nrc-cnrc.gc.ca/en/search/?collection=JCMT&Observation.instrument.name=SCUBA-2&Plane.calibrationLevel=2&noexec=true> [Accessed 24 Mar. 2023].
- [2] JCMT-EAO (n.d.). *SCUBA-2 Integration Time Calculator – James Clerk Maxwell Telescope*. [online] East Asian Observatory. Available at: <https://www.eaobservatory.org/jcmt/instrumentation/continuum/scuba-2/itc/> [Accessed 24 Mar. 2023].
- [3] JCMT-EAO (n.d.). *About the JCMT – James Clerk Maxwell Telescope*. [online] East Asian Observatory. Available at: <http://www.eaobservatory.org/jcmt/about-jcmt/> [Accessed 24 Mar. 2023].
- [4] “Jupiter.” *Lco.global*, lco.global/spacebook/solar-system/jupiter/.
- [5] Robitaille, T., Beaumont, C., McDonald, B. and Rosolowsky, E. (2013). *Astronomical Dendrograms in Python — astrodendro 0.2.0 documentation*. [online] dendrograms.readthedocs.io. Available at: <https://dendrograms.readthedocs.io/en/stable/> [Accessed 16 Mar. 2023].